NASA Technical Memorandum 83143

NASA-TM-83143 19810019010

WIND-TUNNEL EVALUATION OF NASA DEVELOPED CONTROL LAWS FOR FLUTTER SUPPRESSION ON A DC-10 DERIVATIVE WING

I. ABEL AND J. R. NEWSOM

JUNE 1981

National Aeronautics and Space Administration

Langley Research Center
Hampton, Virginia 23665

WIND-TUNNEL EVALUATION OF NASA DEVELOPED CONTROL LAWS FOR FLUTTER SUPPRESSION ON A DC-10 DERIVATIVE WING

I. Abel* and J. R. Newsom**
NASA Langley Research Center
Hampton, Virginia

Abstract

Two flutter suppression control laws have been synthesized, implemented, and tested on a low-speed aeroelastic wing model of a DC-10 derivative. The methodology used to design the control laws is described. Both control laws demonstrated increases in flutter speed in excess of 25 percent above the passive wing flutter speed. The effect of variations in gain and phase on the closed-loop performance was measured and is compared with analytical predictions. In general, the analytical results are in good agreement with experimental data.

Introduction

In order to accelerate new energy efficient technology for both derivative and future commercial transports, NASA is sponsoring an Aircraft Energy Efficiency Program (ACEE). A portion of this effort is aimed at advancing active controls technology. As a participant in the ACEE program, the Douglas Aircraft Company has recently built and tested an aeroelastic wing model of a DC-10 derivative equipped with an active control system.[1]

A considerable effort has been made within NASA advancing active flutter suppression concepts through analytical, wind-tunnel, and flight studies (for example, see Refs. 2 and 3). Because of this extensive background, cooperative studies were initiated to study alternate flutter suppression control laws to be tested on the DC-10 aeroelastic model. The scope of this cooperative study was to apply control law design methods developed by NASA to a realistic transport with engines on the wing and to provide a rapid transfer of technology to industry.

The purpose of this paper is to report on the control laws that were designed at NASA for the DC-10 aeroelastic model and to present results of wind-tunnel tests used to evaluate their performance. The design objective was to synthesize control laws that would demonstrate at least a 20 percent increase in flutter speed over that of the passive wing. The predicted sensitivity of the control laws to both gain and phase is compared with experiment. In addition, a general description of the synthesis methodology is presented.

Although not designed to reduce gust loads, one of the flutter suppression control laws provided substantial gust load alleviation. Reference 4 presents a comparison of analytical and experimental gust response results for this control law.

*Aerospace Engineer, Loads and Aeroelasticity Division
**Aerospace Engineer, Loads and Aeroelasticity Division

Nomenclature

a	control law #1 gain parameter
g	acceleration in gravitational units
K_f	control law #2 gain parameter
K_g	fraction of nominal gain
K_p	phase control filter gain
s	Laplace variable
V	free-stream velocity
V_f	free-stream velocity at flutter
$\ddot{Z}$	feedback acceleration
δ_a	control surface deflection
δ_c	control law command to actuator
ζ	viscous damping coefficient
ζ_n	damping coefficient associated with control law #1
ϕ	phase angle as determined by Eq. (10)
ϕ_m	phase margin
τ	phase control filter time constant
ω	circular frequency
ω_n	circular frequency associated with control law #1

DC-10 Model

The aeroelastic model is representative of a wing which has a 4.27 m span increase over the standard DC-10 wing. The semi-span model is cantilevered from the tunnel wall and has an outboard aileron which is used as the active control surface. A plan view drawing and photograph of the model installed in the wind tunnel is presented in Fig. 1. Results of previous tests of active control laws designed at the Douglas Aircraft Company for flutter suppression and gust load alleviation are given in Ref. 1.

Structure

The model is of conventional spar and pod construction. That is, an aluminum spar is used to provide bending and torsional stiffness with spanwise sections or pods constructed of balsa wood and mylar to provide aerodynamic contours. The engine is represented by a flow-through nacelle and is attached to the wing spar with a beam which provides the pylon the desired degrees of freedom. Although the model was designed to simulate different fuel conditions (through the addition of mass to the wing) all of the present studies were performed for the no-fuel case. For aeroelastic analysis purposes, the first 10 calculated elastic mode shapes, frequencies, and generalized masses were provided to NASA by Douglas Aircraft. The natural frequencies and description of the first 10 modes are presented in Table 1. All modes, except the first three, were assumed to have a structural damping coefficient ζ of 0.01. From ground vibration tests, structural damping in the first three modes was estimated to be 0.0060, 0.0005, and 0.0035, respectively.

Control Surface and Actuator

The model is equipped with a trailing-edge control surface. The control surface is located between the 66.2 percent and 95.5 percent semi-span stations and is approximately 25 percent of the local wing chord. The control surface is driven by an electrohydraulic servo-actuator system. The servo-actuator serves two purposes: for no command it fixes the control surface position relative to the wing (for passive testing); and for time varying inputs, it provides control surface motion in a manner dictated by the control law. Maximum control surface rotation is approximately ±15°.

The actuator servo system was designed with position feedback and is described in Ref. 1. Due to problems in the actuator hardware, tests on the model were performed during two different time periods. In the time interval between the tests, the actuator was modified to improve its reliability. The modifications resulted in differences in the response characteristics of the actuator between the two test periods. Prior to both wind-tunnel entries the actuator frequency response was experimentally measured. For analysis purposes, the measured frequency responses were approximated by a transfer function in the Laplace plane. The measured and approximated frequency responses of the actuator for the two wind-tunnel entries are presented in Fig. 2. Note that the measured phase lag at 12 Hz is approximately 7° greater for the second tunnel entry. The equations used to approximate the measured frequency responses are:

$$\frac{\delta_a}{\delta_c} = \frac{0.6226 \times 10^8}{(s^2 + 180.9\,s + 90958.2)(s + 684.87)} \frac{\text{deg}}{\text{deg}} \qquad (1)$$

Entry 1

$$\frac{\delta_a}{\delta_c} = \frac{1.1105 \times 10^{10}}{(s^2 + 87.51\,s + 138406)(s^2 + 351.6\,s + 75696)} \frac{\text{deg}}{\text{deg}}$$

Entry 2 (2)

Passive Wing Flutter Characteristics

Unsteady aerodynamic forces for the first 10 structural modes and a control surface rotation mode were computed using a doublet lattice aerodynamic computer program. For analysis purposes the structure, the control surface actuator transfer function (for closed-loop analyses), and the unsteady aerodynamics are combined by approximating the variation in frequency of the unsteady aerodynamics with a rational polynomial in the variable s. A description of this analysis method is presented in Ref. 5.

A root locus of the eigenvalues of the characteristic flutter equation as a function of velocity is presented in Fig. 3 (arrows indicate increasing velocity). Each curve corresponds to a structural degree of freedom. The passive wing exhibits two distinct flutter modes as shown in Fig. 3. The first flutter mode occurs at a velocity of 46.93 m/s and is characterized by a coupling between first wing bending (mode 1) and first wing torsion/engine pitch (mode 3). The flutter frequency is approximately 12.5 Hz. The higher frequency flutter mode involves primarily second wing torsion (mode 8) and is stable to a relatively high velocity of 67.1 m/s. The corresponding flutter frequency is approximately 24 Hz.

All experimental studies were conducted in the Douglas Low-Speed Wind Tunnel at Long Beach, California. In the initial phase of testing, the passive flutter characteristics of the wing were determined. Both the damping of the critical flutter mode (mode 3 on Fig. 3) at subcritical speeds and the velocity at flutter were measured. The damping at subcritical speeds was determined by measuring the time to half amplitude of the response of the wing to a pulsed input. (The pulsed input was introduced to the model through small diameter cables which attached to the wing tip and engine nacelle.) A comparison of measured and predicted flutter mode damping (mode 3) is presented in Fig. 4. The predicted flutter velocity is 3 percent lower than measured ($V_{f_{measured}}$ = 48.35 m/s). Estimates of subcritical damping are quite reasonable. Based on these results it appears that the analytical predictions compare reasonably well with the experimental data.

Control Laws

The objective of the study was to design and test control laws capable of demonstrating at least a 20 percent increase in flutter speed over that of the passive wing. The design point selected for control law synthesis was V = 56.32 m/s ($1.2 \times V_f$). Two control laws, one patterned after the aerodynamic energy method and the other after optimal control theory, were designed (for an earlier application of these methods, see Ref. 2). Before proceeding with a brief description of the synthesis methods, those elements common to both control laws will be described.

Early in the design cycle it was decided to move the feedback acceleratometer inboard from the tip where it was located for the tests described in Ref. 1. It was shown experimentally in Ref. 1 (and by analysis preceeding the present design) that to make the control law of Ref. 1 more effective in the 12.5 Hz flutter mode an increase in system gain would be required. This increased gain however, destabilizes the third wing bending mode resulting in an instability at 34.7 Hz (see Fig. 12, Ref. 1). To decouple this mode from the flutter suppression system, the feedback accelerometer was moved inboard to a point close to the node line associated with third wing bending. Both control laws used this location for the feedback accelerometer.

In order to eliminate any static gain problems, such as a DC drift in the accelerometer amplifier,

a "washout" filter of the form $s/(s + 5)$ was added to the feedback loop prior to control law synthesis. In addition, both control laws were designed using the actuator transfer function defined by Eq. (1).

Synthesis

Control Law #1. The form of this control law was patterned after the aerodynamic energy method and used the following transfer function for design purposes:

$$\frac{\delta_a}{\ddot{z}} = \frac{\delta_c}{\ddot{z}} \times \frac{\delta_a}{\delta_c} \quad \frac{deg}{g} \tag{3}$$

where δ_a/δ_c is defined by Eq. (1) and the control law is defined by

$$\frac{\delta_c}{\ddot{z}} = \frac{a}{(s^2 + 2\zeta_n \omega_n s + \omega_n^2)} \times \frac{s}{(s + 5)}$$

The design process, using the aerodynamic energy method, involves determining the values of a, ζ_n, and ω_n which minimizes control surface response to tunnel turbulence. However, a spectrum of tunnel turbulence for the flutter testing portion of the tests was not available. As stated in Ref. 1, a banner was installed in the tunnel to create turbulence for load measurements but the banner was removed for flutter testing. Therefore, the design process involved determining the values of these three parameters which provides the required increase in flutter speed with acceptable gain and phase margins across the velocity range. For this study gain margins of ±6 dB and phase margins of ±30° were selected. The values of a, ζ_n, and ω_n which satisfied these requirements were determined by trial and error.

An example of the effect of varying the gain parameter "a" on flutter mode damping is presented in Fig. 5a. For this case the parameters ζ_n and ω_n were fixed at 1.0 and 25 rad/s, respectively as previously determined by trial and error. The dotted line represents the passive wing damping characteristics in this mode. (Note that the value of structural damping at $V = 0$ in Fig. 5a is larger than that presented previously in Fig. 4. During control law synthesis the structural damping in mode 3 was erroneously assumed to be 0.0064. The effect of this difference on the design will be discussed later.) It can be seen from Fig. 5a that the closed-loop damping at velocities below the passive wing flutter speed has been reduced. This occurred for all combinations of a, ζ_n and ω_n that were analyzed. Since the level of damping in the passive wing flutter mode is very low to begin with ($\zeta_{max} \approx 0.0085$), it was decided that a constraint based on damping would be added to the design. The constraint was that for nominal gain the minimum closed-loop damping below the passive wing flutter speed could not be lower than the structural damping at zero velocity (i.e., $\zeta_{min} \geq \zeta_{wind\ off}$). The curve represented by $a = 8.449 \times 10^3$, $\zeta_n = 1.0$ and $\omega_n = 25$ came the closest the meeting the design requirements. Figure 5b presents a Nyquist diagram of this control law at the design point ($V = 56.32$ m/s). Arrows indicate increasing frequency. Gain margins of -8.1 dB and 5.8 dB along with phase margins of -75° and +45° are indicated. The following transfer function represents the control law (which includes the washout filter) that was implemented on the model:

$$\frac{\delta_c}{\ddot{z}} = \frac{8.449 \times 10^3}{(s^2 + 50\ s + 625)} \times \frac{s}{(s + 5)} \quad \frac{deg}{g} \tag{4}$$

Control Law #2. The synthesis technique used to design control law #2 is based on the method described in Ref. 2. This method is used to design a reduced order control law from the results of a full-state feedback optimal control law. The method requires that the open-loop frequency response of the reduced order control law closely match the open-loop frequency response of the full-state optimal control law over a finite frequency range.

The form of the control law initially examined was similar to control law #1, that is

$$\frac{\delta_c}{\ddot{z}} = \frac{K_f}{(s^2 + 2\zeta_n \omega_n s + \omega_n^2)} \times \frac{s}{(s + 5)} \tag{5}$$

An optimization algorithm was then used to find the values of K_f, ζ_n, and ω_n that minimize the difference between the open-loop frequency response using Eq. (5) and the optimal open-loop frequency response at the design point. The optimization algorithm drove ζ_n and ω_n to zero resulting in

$$\frac{\delta_c}{\ddot{z}} = \frac{K_f}{s^2} \times \frac{s}{(s + 5)} \tag{6}$$

This control law results in high system gain at low frequency and therefore, the s^2 term was arbitrarily changed to $(s + 10)^2$ resulting in the following control law

$$\frac{\delta_c}{\ddot{z}} = \frac{K_f}{(s + 10)^2} \times \frac{s}{(s + 5)} \quad \frac{deg}{g} \tag{7}$$

where $K_f = 4.45 \times 10^3$. A Nyquist diagram of this control law at the design point is presented in Fig. 6a. As shown in this figure, the gain and phase margins at the design point are acceptable. The flutter mode damping across the velocity range, using this control law, is presented in Fig. 6b. Note that this control law drives the wing unstable below the passive wing flutter speed. This is attributed to the fact that the optimal control law at the design point requires 180° of phase lag. This amount of phase lag at velocities below the passive wing flutter speed promotes the instability. Further analysis indicated that the addition of 30° of phase lead (at 12 Hz) to Eq. (7) eliminates the instability. However, the addition of this phase lead significantly reduces the positive gain margin. Therefore, the terms that were added to improve both the flutter mode damping and gain margins of the control law are as follows:

(1) $\frac{(s - 20)}{(s + 20)}$

approximately 30° of phase lead at 12 Hz to improve flutter mode damping near the passive wing flutter speed.

(2) $\frac{(s^2 + 7.2\ s + 144)}{(s^2 + 19.2\ s + 144)}$

notch filter at approximately 2 Hz to improve the positive gain margin resulting from the introduction of (1).

(3) $\frac{628^2}{(s + 628)^2}$

a 100 Hz double pole filter to eliminate high frequency inputs.

(4) An increase in K_f (from 4.45×10^3 to 6.64×10^3) to compensate for a decrease in the negative gain margin resulting from the introduction of (1), (2), and (3).

The resulting control law can be written as

$$\frac{\delta_c}{\ddot{Z}} = \frac{6.64 \times 10^3}{(s + 10)^2} \times \frac{s}{(s + 5)} \times \frac{(s - 20)}{(s + 20)}$$

$$\times \frac{(s^2 + 7.2\ s + 144)}{(s^2 + 19.2\ s + 144)} \times \frac{(628)^2}{(s + 628)^2} \frac{\text{deg}}{g} \qquad (8)$$

The Nyquist diagram at the design point using Eq. (8) is presented in Fig. 7a. Comparing these results to those in Fig. 6a, it can be seen that at the design point the stability margins have decreased but are still within the acceptable region. The flutter mode damping as a function of velocity is presented in Fig. 7b. Comparing these results with those of Fig. 6b, the improvement in flutter mode damping can be seen and the wing remains stable throughout the velocity range of interest.

Implementation

A simplified block diagram of both flutter suppression systems is presented in Fig. 8. Both control laws were programmed on a COMCOR 175 analog computer. The analog computer processes the feedback accelerometer output signal from the wing and, based on the control law being tested, determines the appropriate actuator command signal. To evaluate the effect of phase on the stability characteristics of each control law a filter of the form

$$K_p \frac{(1 - \tau s)}{(1 + \tau s)} \qquad (9)$$

where

$K_p = +1$ for phase lag

$K_p = -1$ for phase lead

was programmed on the analog computer. For a given phase angle at circular frequency ω (where $s = i\omega$), the time constant τ is evaluated by the equation

$$\tau = \tan ((1 - K_p) \times 45 - \phi/2)/\omega \qquad (10)$$

where ϕ is in degrees. Both gain and phase were varied during the wind-tunnel tests and these results will be compared to analytical predictions.

Predicted Performance

As mentioned previously, the wind-tunnel studies were performed during two different tunnel entries. During the first entry both control laws were tested to establish their effects on raising the passive flutter speed. During a series of runs to establish the effect of gain and phase on the performance of the control laws, servo-actuator problems resulted in termination of the first wind-tunnel test. During the second tunnel entry control law #1 was thoroughly evaluated in terms of gain and phase. Control law #2 was not tested during the second tunnel entry. As stated previously, both control laws were designed assuming the damping in mode 3 to be $\zeta = 0.0064$. It was determined that the damping in this mode was actually 0.0035. The predicted performance will take into account the actuator frequency response applicable to the test entry and the corrected value of structural damping in the flutter mode.

Control Law #1. Figure 9 presents Nyquist diagrams of control law #1 with the lower value of structural damping in mode 3 (Fig. 9a) and with the modified actuator (Fig. 9b). A summary of these results is presented in the following table:

Descript.	Gain margin dB	Gain margin dB	ϕ_m deg	ϕ_m deg	ζ_3/Actuator
Pre-test	-8.1	5.8	-75	45	0.0064/Eq. (1)
Entry 1	-5.6	4.3	-62	31	0.0035/Eq. (1)
Entry 2	-6.8	1.5	-78	12	0.0035/Eq. (2)

The predominant effect of reducing ζ_3 is to decrease both the gain and phase margins. The modified actuator transfer function tends to rotate the Nyquist diagram clockwise about the origin. This results in a significantly lower positive phase margin and a lower positive gain margin. These results indicate the need for an accurate definition of the actuator frequency response prior to beginning the design process. In addition, since this model has such low damping in the flutter mode it is important that the magnitude of the structural damping term be established early in the design cycle. Since the bulk of experimental data on control law #1 was gathered during the second tunnel entry, the predicted results for this case will be presented (i.e., $\zeta_3 = 0.0035$; actuator transfer function Eq. (2)).

Using the control law defined by Eq. (4) and the actuator transfer function defined by Eq. (2), a stability calculation was performed. The results of this calculation are presented in Fig. 10 as a closed-loop root locus which illustrates the variation of the modal eigenvalues of the system with velocity (arrows indicate increasing velocity). Comparing these results with those of the passive system (Fig. 3), we note the following: (1) the flutter mode (mode 3) is stabilized to the maximum velocity analyzed (V = 76.2 m/s); (2) modes 2, 5, 6, 7, 9, and 10 are basically unaffected by the active control system; (3) mode 8 is unstable at V = 0; it becomes stable at low values of V, and then goes unstable once again at approximately the same value of V as the passive wing; (4) two new modes associated with the feedback filter and actuator are generated. The instability in mode 8 at V = 0 becomes stable at velocities well below any test conditions.

The variation in flutter mode damping (ζ_3) with velocity at various values of gain and phase is presented in Fig. 11. The term K_g is a multiplying factor used with Eq. (4) and can be considered as the fraction of nominal gain for which the system is analyzed. (For example, $K_g = 1.0$ refers to nominal gain or $a = 8.449 \times 10^3$; $K_g = 0.2$ would be equivalent to $a = 1.690 \times 10^3$; and $K_g = 0$ is the passive wing case). The phase angle ϕ refers to the value of the phase control filter (Eq. (10)) evaluated at 12.5 Hz. The damping characteristics of the nominal control law ($\phi = 0°$; $K_g = 1.0$) is presented in Fig. 11a. All analyses were performed to a maximum velocity of 76.2 m/s. However, the curves in Fig. 11 are terminated when a mode (other than mode 3) goes unstable. For example, at nominal phase and gain mode 3 is stable to a velocity beyond V = 76.2 m/s but at V = 65.5 m/s mode 8 becomes unstable (see Fig. 10) and the curve is terminated. Figures 11b and 11c follow the same format but for phase angles of -20° and +20°, respectively.

It can be seen in Fig. 11a that the nominal control law provides an increase in velocity above the passive wing in excess of 20 percent. However, as mentioned previously, due to the decrease in structural damping in the flutter mode and the actuator modifications the control law does not exhibit either the ±6 dB gain margins or the ±30° phase margins. For all phase angles analyzed the control law degrades the flutter mode damping at low velocities. This degradation is less for the positive phase angles and greater for the negative phase angles. As velocity is increased this trend is reversed. The effect of phase angle on system performance is attributed to significant phase variations in the response of the wing to control surface motion that are experienced as the velocity is increased. This fact coupled with the extremely low value of damping in the flutter mode for this wing results in a control law which is very sensitive to phase variation. These results indicate that a control law which includes phase scheduling with velocity would have damping characteristics superior to a constant coefficient system. The concept of phase scheduling was beyond the scope of this investigation.

Control Law #2. Since all of the experimental data for control law #2 was gathered during the first tunnel entry, the predicted results for this case will be presented (i.e., $\zeta_3 = 0.0035$; actuator transfer function Eq. (1)). Figure 12 presents the Nyquist diagram at the design point (V = 56.32 m/s) using control law #2. The predominant effect of reducing ζ_3 is to decrease the negative phase and negative gain margins.

The variation of flutter mode damping (ζ_3) with velocity at various values of gain and phase is presented in Fig. 13. The format for this figure is the same as previously described for control law #1 (i.e., K_g, ϕ, and maximum velocity plotted). The nominal control law provides an increase in velocity above the passive wing flutter speed in excess of 20 percent. The trends with phase angle and gain for control law #2 are similar to that presented for control law #1. However, it should be noted that the phase angles presented in Fig. 13 are ±10° as compared to ±20° for control law #1. Comparing the variation in flutter mode damping for both control laws (Figs. 11 and 13), it can be seen that the effect of phase lead on control law #2 is greater than for control law #1. This is attributed to the fact that control law #1 has a larger negative phase margin at the design point than control law #2 (-78° as compared to -44°). Positive phase introduced by the phase control filter rotates the Nyquist diagram in a counterclockwise direction. Since control law #1 has a larger negative phase margin, phase lead will have less of an effect on this control law. Calculations performed for control law #2 with 20° of phase lead predicted that the closed-loop system would be unstable. For all phase angles analyzed, the control law degrades the flutter mode damping at low velocities. This degradation is less for the positive phase angles than for the negative angles. As velocity is increased, this trend is reversed.

Wind Tunnel Results and Comparison With Analysis

Control Law #1

As stated previously, this control law was tested during both tunnel entries. Since the majority of the data were acquired during the second entry, only a qualitative description of the results acquired during the first entry is presented. The tendency of the flutter suppression system to reduce damping in the flutter mode prior to the passive wing flutter speed (see Fig. 11a for $K_g = 1.0$) was visually observed during the tests. As the passive wing flutter speed was approached, the closed-loop damping appeared to be quite low. As the tunnel velocity was increased beyond the passive flutter speed, the model appeared to be quite stable. A phase lead of 30° was added to the control law using the phase control filter. For this phase lead the damping of the closed-loop system near the passive wing flutter speed was significantly improved, as predicted by analysis. Prior to the first run, the feedback loop was closed and the model was excited with a pulsed input. As predicted, mode 8 was unstable at a frequency of approximately 42 Hz. Repeated excitation of the model at the lowest test velocity (15.4 m/s) demonstrated that this mode does become stable as predicted.

Prior to the second tunnel entry the analysis presented in Fig. 11 was performed. As a result of this calculation it was determined that phase lags introduced by modifying the actuator would result in a flutter suppression system that would have degraded performance. In fact, when the control law was tested at nominal phase and gain the system was unstable below the passive wing flutter speed. To account for the extra phase lag introduced by the modified actuator (approximately 7° at 12.5 Hz), a phase lead of +10° was introduced into the feedback system with the phase control filter. The resulting system behaved in a manner quite similar to that observed during the first entry.

Calculated stability boundaries in terms of flutter velocity versus system gain for six values of phase that were evaluated during the second tunnel entry are presented in Fig. 14. Three or four distinct flutter modes are exhibited, depending on phase angle. For all phase angles analyzed, a decrease in flutter velocity is shown for mode 3 at low values of gain. At negative phase angles, the reduction in flutter velocity is more pronounced. The velocity at which mode 8 goes unstable is nearly independent of system gain and phase. The mode 4 instability is aggravated by negative phase angles and stays relatively fixed for positive phase angles. At phase angles of +20° and above a new flutter mode resulting from a coupling between the feedback filter mode and the first wing bending mode becomes critical. It should be noted that the phase angles in Fig. 14 correspond to Eq. (10) evaluated at $\omega = 78$ rad/s. The phase angle produced by the phase control filter at other frequencies is significantly different.

Also presented in Fig. 14 is the experimental data measured during the test. Two correction factors have been applied to the experimental data and will be described before comparing the results with analysis. The first correction factor applies to system gain. It was stated in Ref. 1 that computed aileron forces were typically 40 percent higher than measured quantities. When a correction factor was used to account for this difference, the response of the wing due to control surface motions was predicted with better accuracy. Therefore, this correction factor will be used in the present comparison. Since system gain is directly proportional to control surface effectiveness, a correction factor of 0.714 (= 1/1.4) was used for the experimental data before comparing it to the analytical data (i.e., a gain setting of $K_g = 1.0$ experimentally will be plotted at $K_g = 0.714$). The second correction factor deals with phase angle. Prior to most of the flutter runs during the second tunnel entry, a check of the system gain and phase characteristics was performed. This was done by removing the feedback accelerometer signal from the analog computer and replacing it with a sine wave of known frequency and amplitude. This signal was used to drive the control surface. The amplitude and phase of the control surface motion to the input signal was then determined using a signal analyzer. At 12 Hz the predicted phase lag of the response with respect to input was 163°. For $\phi = 0°$ (phase control filter) the measured phase lag was approximately 172°. Therefore, the experimental data will be compared to a nominal phase angle of -163°. (For example, for the phase control filter set to 0° the experimental data used in the comparison will be $\phi = -10°$). With these correction factors applied to the experimental data, the comparison of experimental results and predictions presented in Fig. 14 are quite good as is indicated by the following:

(1) the tendency of mode 3 to be destabilized below the passive flutter speed for all phase angles at low values of gain. This effect is more pronounced at negative phase angle;

(2) the tendency of phase lead to improve the mode 3 flutter characteristics at low velocities and to have the opposite effect at higher velocities;

(3) the existence of a mode 4 instability at $\phi = -10°$; and

(4) the existence of a coupled filter first wing bending mode at a phase lead of +30°.

From the data presented in Fig. 14, it can be shown that increases in flutter speed in excess of 25 percent were demonstrated at phase angles of 0°, +10°, +20°, and +30°.

Control Law #2

This control law was tested only during the first tunnel entry. Data are only available for gain variations at nominal phase since control law #2 was not tested as thoroughly as control law #1.

Figure 15 presents the calculated stability boundary in terms of flutter velocity versus system gain for nominal phase ($\phi = 0°$). Results in general follow the same pattern as control law #1. The model exhibited a decrease in flutter velocity for mode 3 at low values of gain. As gain is increased, the flutter velocity for mode 3 increased and the critical flutter mode became mode 8. The velocity at which mode 8 became unstable is nearly independent of system gain. Also presented in Fig. 15 are the experimental data measured during the test. The correction for the computed control surface forces described previously is also applied here. With the correction factor the comparison of experimental results and predictions are quite good. As indicated in Fig. 15, an increase in flutter speed in excess of 25 percent was also demonstrated for control law #2.

Conclusions

This paper presents the results of an experimental evaluation of control laws designed to suppress flutter of a DC-10 derivative aeroelastic wing model. Two control laws were synthesized and tested on the model in the Douglas Long Beach low-speed wind tunnel. Both control laws increased the passive wing flutter speed in excess of 25 percent. Qualitative measurements and analytical predictions indicate that both control laws reduce the flutter mode damping at velocities below the passive flutter speed. Gain margins and phase margins were less than desired; however, it is believed that with another design iteration that takes into account the changes in the servo-actuator and structural

damping, that were experienced, these margins can be improved. Other significant conclusions are:

(1) Analytically derived control laws using the methods described herein, were capable of demonstrating large increases in flutter speed without the necessity of modifying the control laws during the wind-tunnel tests.

(2) Calculations performed prior to wind-tunnel testing predicted the flutter mode damping trends.

(3) The use of correction factors to account for control surface effectiveness and for measured phase differences in the experimental system resulted in good correlation between measured and predicted flutter boundaries as a function of gain and phase.

Acknowledgement

The authors wish to acknowledge the work of E. Tescher, J. Nomura, J. Schlama, and A. Shirley of the McDonnell Douglas Corporation. The successful completion of this study was due largely to their skillful efforts in conducting the wind-tunnel tests and acquiring the experimental data.

References

[1]Winther, B. A.; Shirley, W. A.; and Heimbaugh, R. M.: Wind Tunnel Investigation of Active Controls Technology Applied to a DC-10 Derivative. Presented at the AIAA/ASME 21st Structures, Structural Dynamics and Materials Conference, Seattle, WA, May 1980. AIAA Paper No. 80-0771.

[2]Newsom, J. R.; Abel, I.; and Dunn, H. J.: Application of Two Design Methods for Active Flutter Suppression and Wind-Tunnel Test Results. NASA TP-1653, May 1980.

[3]Murrow, H. N.; and Eckstrom, C. V.: Drones for Aerodynamic and Structural Testing (DAST) - A Status Report. J. Aircraft, Vol. 16, No. 8, August 1979, pp. 551-556.

[4]Perry, B., III: Qualitative Comparison of Calculated Turbulence Responses and Wind-Tunnel Measurements of a DC-10 Derivative Wing with an Active Control System. Presented at the AIAA Dynamics Specialists Conference, Atlanta, GA, April 1981. AIAA Paper No. 81-0567.

[5]Abel, I.: An Analytical Technique for Predicting the Characteristics of a Flexible Wing Equipped with an Active Flutter Suppression System and Comparison with Wind-Tunnel Data. NASA TP-1367, 1979.

Table 1 Structural modes of wind-tunnel model

Mode	Description	Frequency, Hz
1	1st wing bending	5.18
2	Engine yaw	6.23
3	1st wing torsion/engine pitch	12.57
4	2nd wing bending	16.29
5	Engine roll	22.97
6	Wing fore and aft bending	23.25
7	3rd wing bending	33.20
8	2nd wing torsion	42.18
9	---	59.10
10	---	62.99

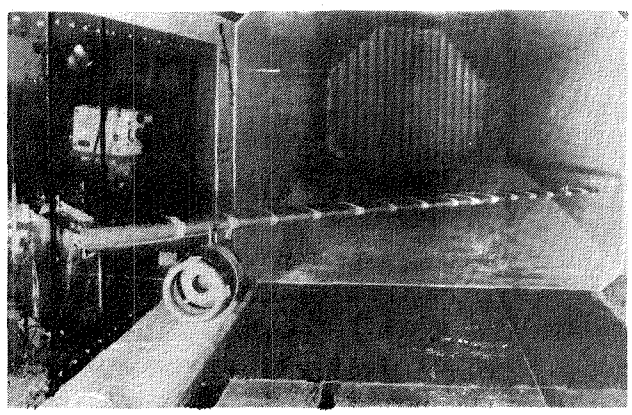

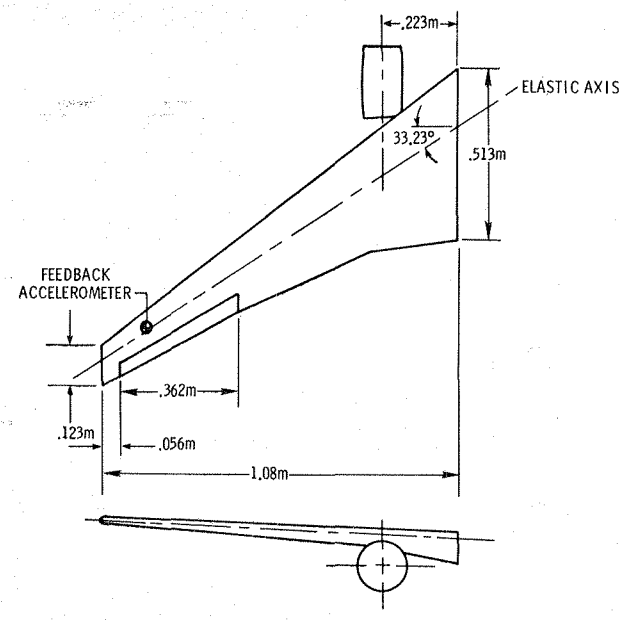

Fig. 1 DC-10 derivative aeroelastic wing model.

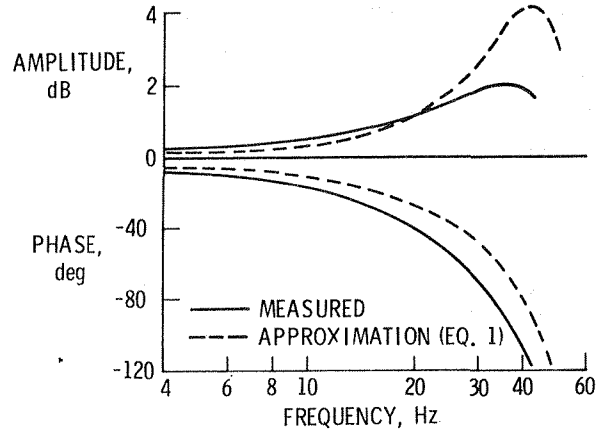

a) First entry.

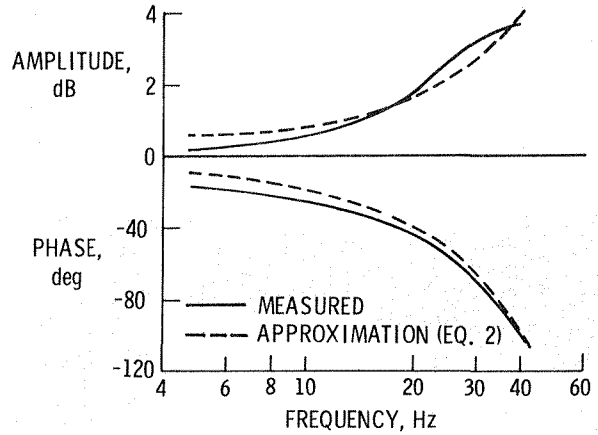

b) Second entry.

Fig. 2 Measured and approximated frequency response of actuator.

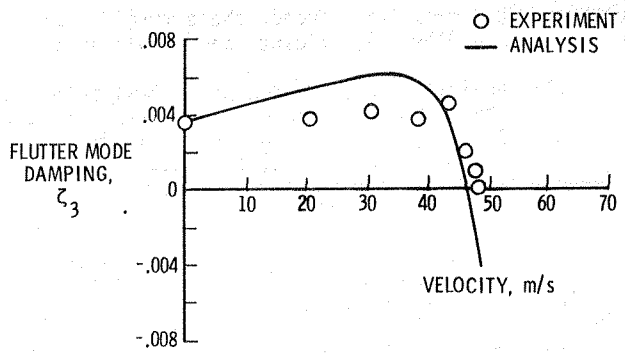

Fig. 4 Comparison of measured and predicted flutter mode damping (passive wing).

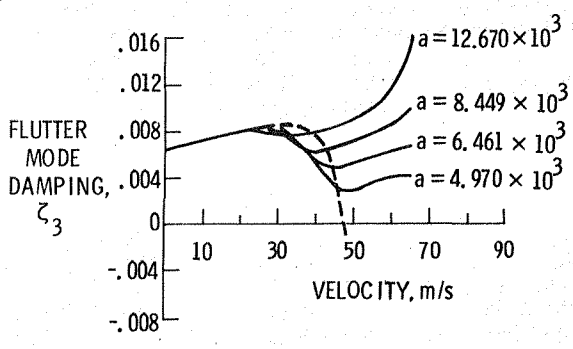

a) Predicted variation in flutter mode damping with gain (ζ_n = 1.0; ω_n = 25 rad/s; actuator defined by EQ. 1).

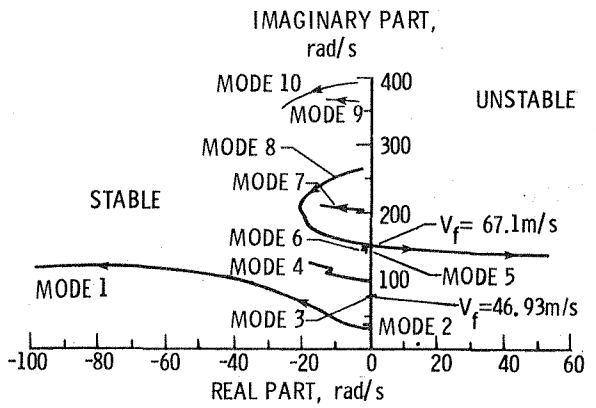

Fig. 3 Velocity root locus (passive wing; arrows indicate increasing velocity).

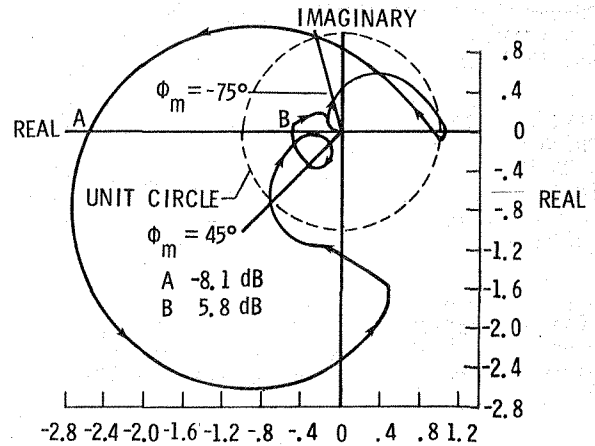

b) Nyquist diagram at V = 56.32 m/s for a = 8.449 x 10^3 (arrows indicate increasing frequency).

Fig. 5 Characteristics of control law #1.

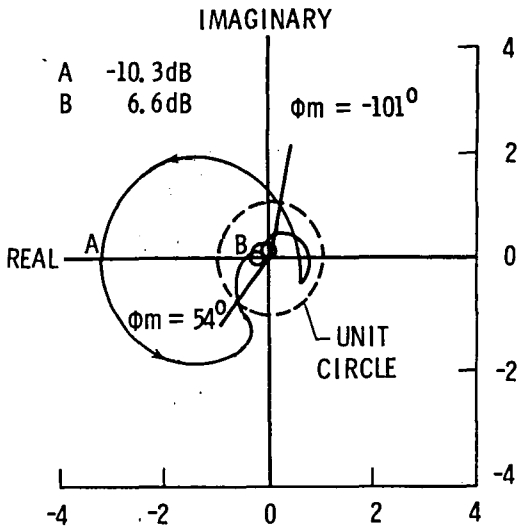

a) Nyquist diagram at V = 56.32 m/s (arrows indicate increasing frequency).

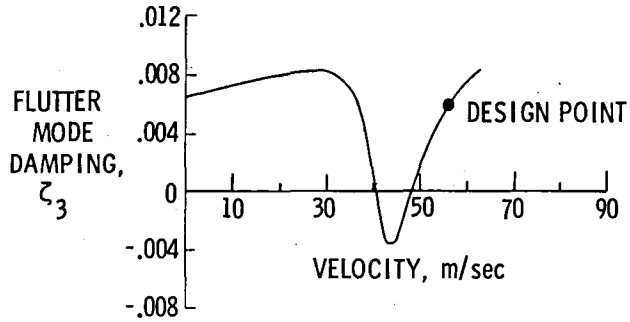

b) Predicted variation in flutter mode damping.

Fig. 6 Characteristics of control law #2 as defined by Eq. (7).

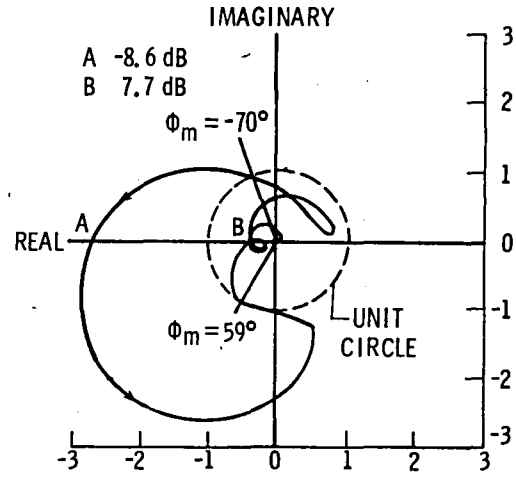

a) Nyquist diagram at V = 56.32 m/s (arrows indicate increasing frequency).

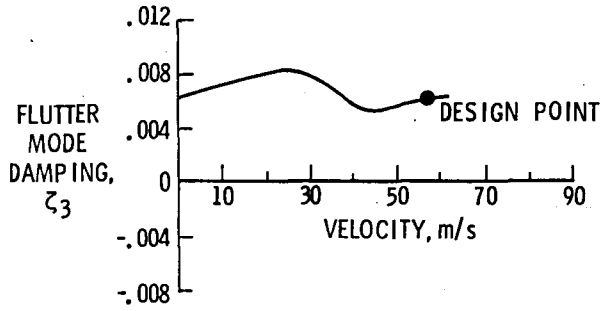

b) Predicted variation in flutter mode damping.

Fig. 7 Characteristics of control law #2 as defined by Eq. (8).

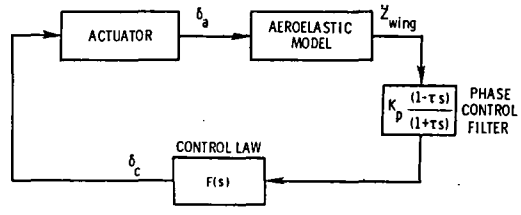

CONTROL LAW 1

$$F(s) = \frac{8.449 \times 10^3}{(s^2+50s+625)} \times \frac{s}{(s+5)} \frac{deg}{g}$$

CONTROL LAW 2

$$F(s) = \frac{2.618 \times 10^9 (s^2+7.25s+144)(s-20)}{(s^2+19.2s+144)(s+10)^2(s+20)(s+628)^2} \times \frac{s}{(s+5)} \frac{deg}{g}$$

Fig. 8 Block diagram of active control system.

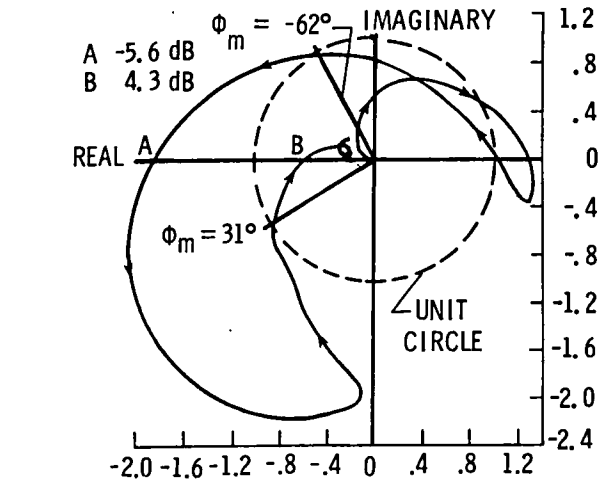

a) ζ_3 = 0.0035; actuator defined by Eq. (1).

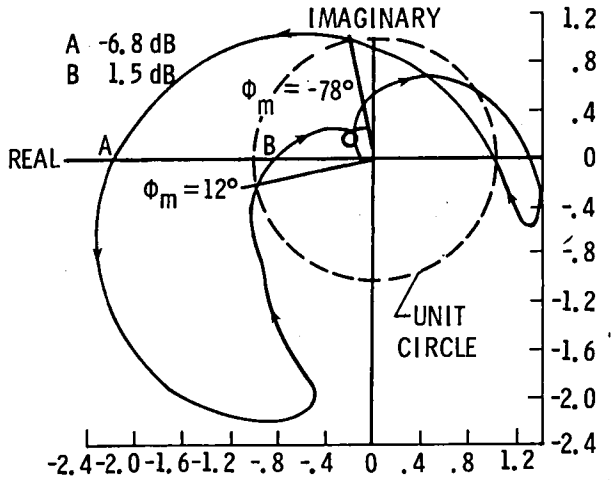

b) ζ_3 = 0.0035; actuator defined by Eq. (2).

Fig. 9 Nyquist diagram of control law #1 at V = 56.32 m/s with modified actuator and ζ_3.

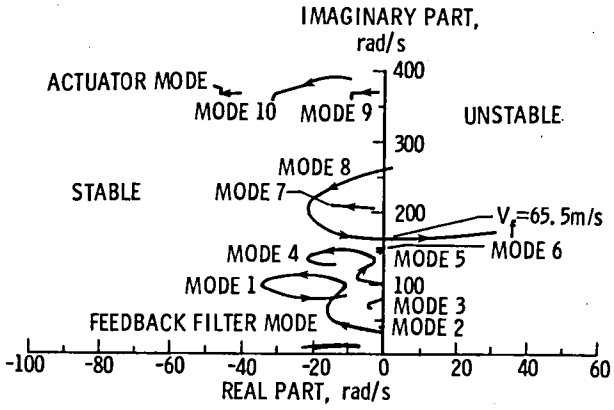

Fig. 10 Closed-loop velocity root locus (control law #1; ζ_3 = 0.0035; actuator defined by Eq. (2)).

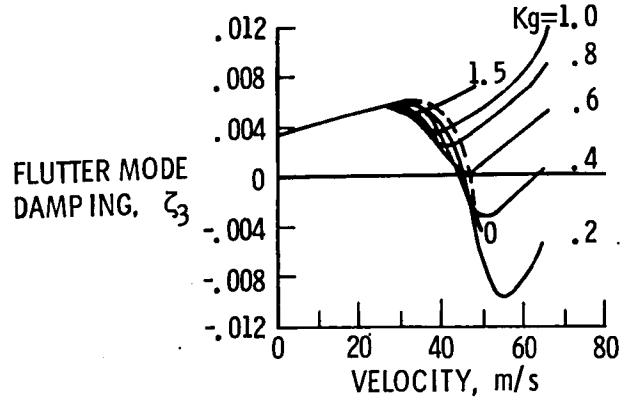

a) ϕ = 0°

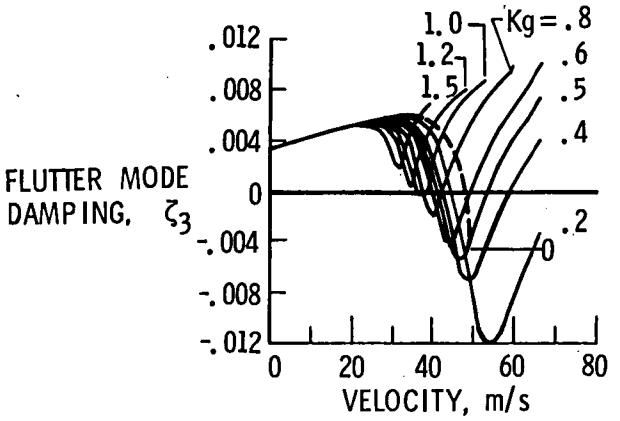

b) ϕ = -20°

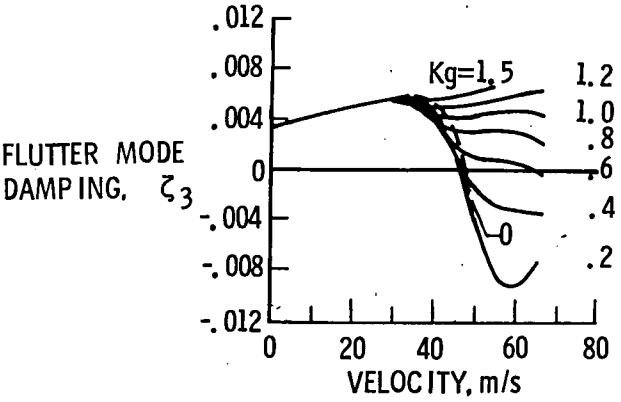

c) ϕ = +20°

Fig. 11 Predicted variation in flutter mode damping with gain and phase (control law #1; ζ_3 = 0.0035; actuator defined by Eq. (2)).

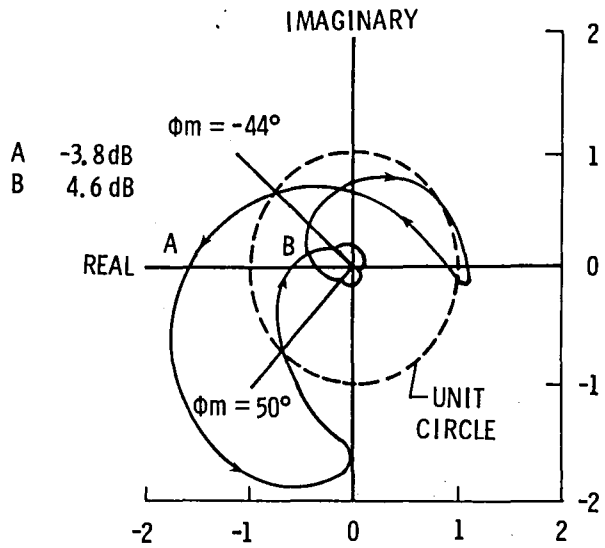

Fig. 12 Nyquist diagram of control law #2 at V = 56.32 m/s with ζ_3 = 0.0035.

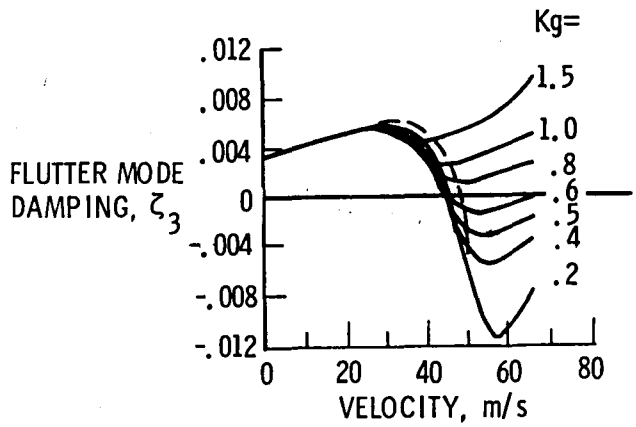

a) $\phi = 0^\circ$

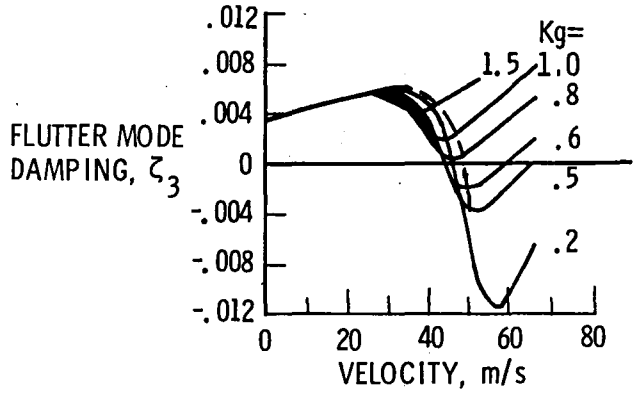

b) $\phi = -10^\circ$

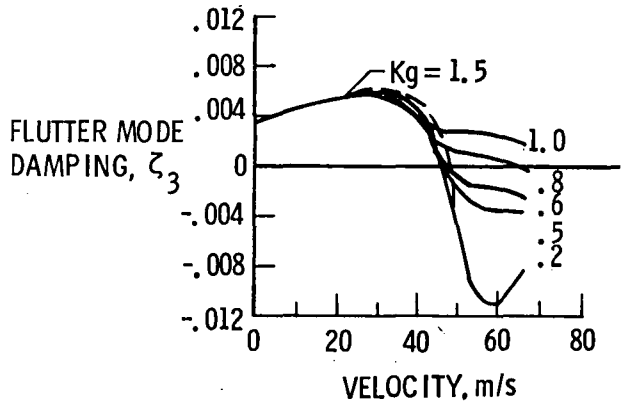

c) $\phi = +10^\circ$

Fig. 13 Predicted variation in flutter mode damping with gain and phase (control law #2; ζ_3 = 0.0035; actuator defined by Eq. (1)).

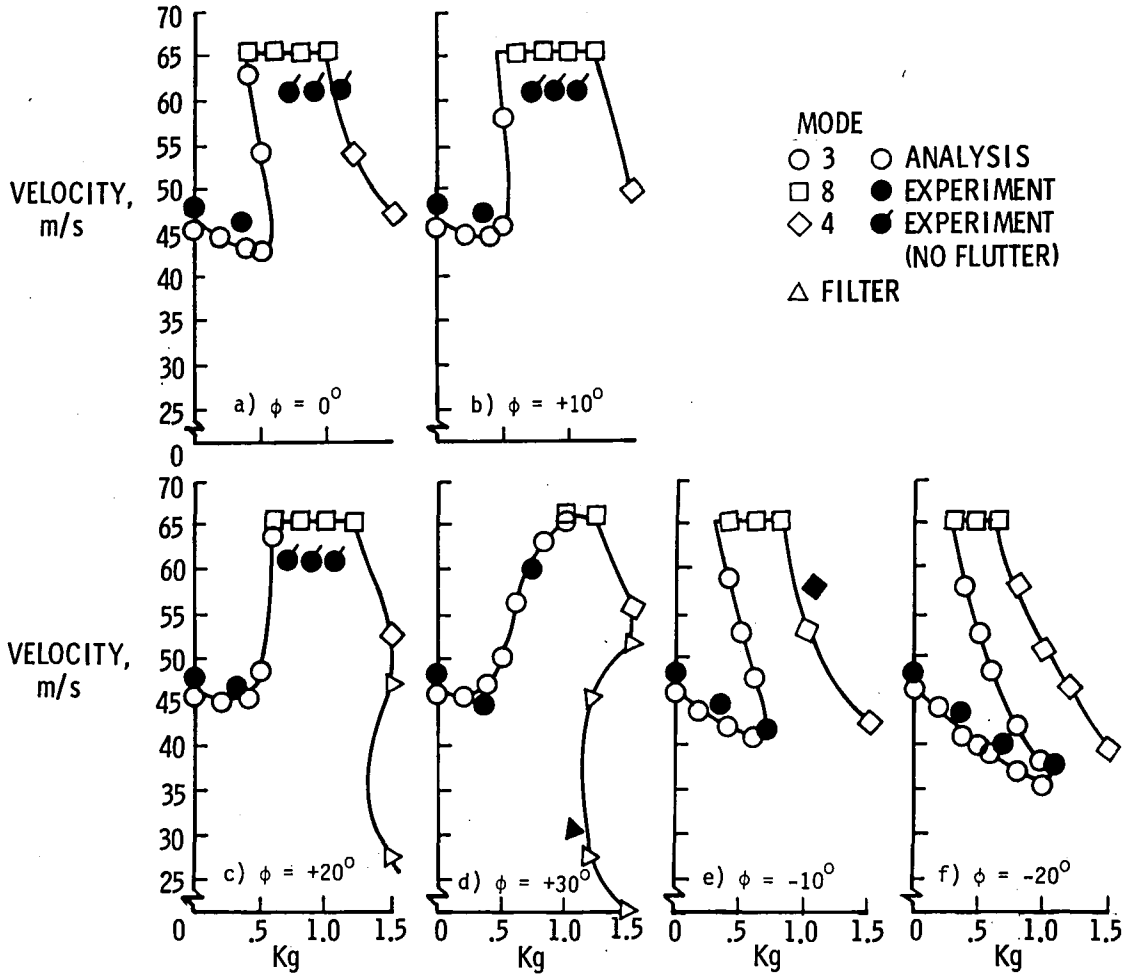

Fig. 14 Measured and predicted stability boundaries as a function of gain and phase (control law #1).

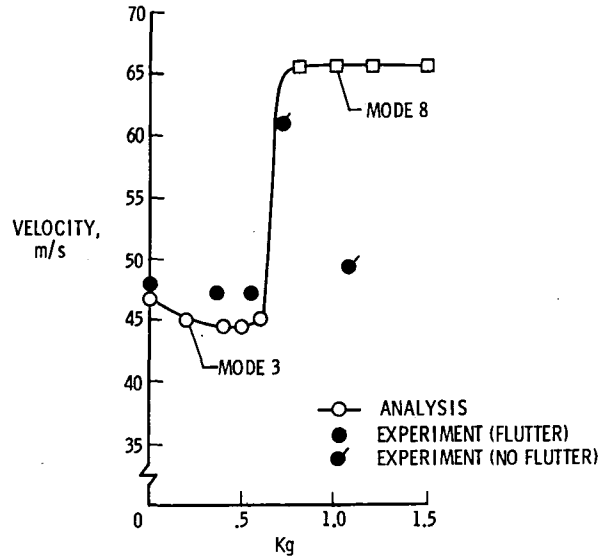

Fig. 15 Measured and predicted stability boundary as a function of gain (control law #2).

1. Report No.	2. Government Accession No.	3. Recipient's Catalog No.
NASA TM-83143		

4. Title and Subtitle	5. Report Date
Wind-Tunnel Evaluation of NASA Developed Control Laws for Flutter Suppression on a DC-10 Derivative Wing	June 1981
	6. Performing Organization Code 505-33-63-02
7. Author(s)	8. Performing Organization Report No.
I. Abel and J. R. Newsom	
	10. Work Unit No.
9. Performing Organization Name and Address	11. Contract or Grant No.
NASA Langley Research Center Hampton, Virginia 23665	
	13. Type of Report and Period Covered
12. Sponsoring Agency Name and Address	Technical Memorandum
National Aeronautics and Space Administration Washington, DC 20546	14. Sponsoring Agency Code

15. Supplementary Notes

Presented at the AIAA Dynamics Specialist Conference, Atlanta, Georgia, April 8-11, 1981. AIAA Paper No. 81-0639.

16. Abstract

Two flutter suppression control laws have been synthesized, implemented, and tested on a low-speed aeroelastic wing model of a DC-10 derivative. The methodology used to design the control laws is described. Both control laws demonstrated increases in flutter speed in excess of 25 percent above the passive wing flutter speed. The effect of variations in gain and phase on the closed-loop performance was measured and is compared with analytical predictions. In general, the analytical results are in good agreement with experimental data.

17. Key Words (Suggested by Author(s))	18. Distribution Statement
Flutter Suppression, Aeroelasticity, Wind Tunnel test	Unclassified - Unlimited Subject category 39

19. Security Classif. (of this report)	20. Security Classif. (of this page)	21. No. of Pages	22. Price
Unclassified	Unclassified	13	A02

End of Document